Population Balance Model for Nucleation, Growth, Aggregation, and Breakage of Hydrate Particles in Turbulent Flow

Boris V. Balakin, Alex C. Hoffmann, and Pawel Kosinski
Dept. of Physics and Technology, University of Bergen, Allegaten 55, Bergen 5007, Norway

DOI 10.1002/aic.12122
Published online December 14, 2009 in Wiley InterScience (www.interscience.wiley.com).

This article describes a computational model for the size evolution of hydrate particles in a pipeline-pump system with turbulent flow. The model is based on the population balance principle, and the simulation results were validated with data from an experimental study of a flow loop containing hydrate particles reported in the literature. It is found that the particle size is significantly influenced by aggregation and breakage, related to shear in the flow, and that these effects are comparable to those of growth and nucleation, related to diffusional processes. Two different approaches for hydrate growth and nucleation, one of continuous nucleation during the process and one of only an initial nucleation-pulse, were used. This was done to compare the aggregation and breakage parameters which come out when fitting the models output to experiment. These two approaches are found to give rise to similar aggregation/breakage parameters, lending credence to the pbm-based modeling. © 2009 American Institute of Chemical Engineers *AIChE J*, 56: 2052–2062, 2010

Keywords: population balance, hydrates, flocculation, breakage, crystal growth, mathematical modeling, multiphase flow

Introduction

Gas hydrates are similar in appearance to ice. They are compounds of water and light molecules, often hydrocarbons, which may be created at temperatures above the freezing point of water at normal conditions. They are ''clathrates'' formed by occupation of cages in a water-crystal structure by ''guest'' molecules,[1] which are not chemically bound to the water crystal. In nature the guest molecules are mainly methane molecules, and such natural gas hydrates may be found in a deep sea floor deposits and under permafrost[1] where water and natural gas are present and the conditions are within their thermodynamic region of stability: high pressure and low temperature. Naturally formed hydrates are thought to constitute a potentially important future energy source when conventional oil and gas resources are exhausted.[2] Gas hydrates may be formed technologically for usage in refrigeration systems,[3] transportation of natural gas in the form of hydrate[4] and water desalination.[5]

On the other hand, hydrates constitute a problem during oil and gas processing and transportation: once hydrate nuclei are formed in a pressurized pipeline they may grow increasing the concentration of solids in the flowing fluid.[1] From the rheological point view the presence of the hydrate particles increases the apparent viscosity of transported media enhancing the frictional pressure loss over the pipeline.[6]

In this context, the determination of hydrate particle size and fractal structure becomes important to predict the rheological behavior of the multiphase mixture.[7] This may be determined statistically using the population balance modeling (PBM) theory developed by Smoluchowski[8] which describes balances for each particle size band, the particles moving into, called a ''birth'' or out of, a ''death'', a given size band due to nucleation, growth, agglomeration and breakage. These size bands may be infinitesimal. The terms ''birth'' and ''death'' stem from the process being viewed and modeled as a birth-death Markov process, but

Correspondence concerning this article should be addressed to B. V. Balakin at boris.balakin@sintef.no.

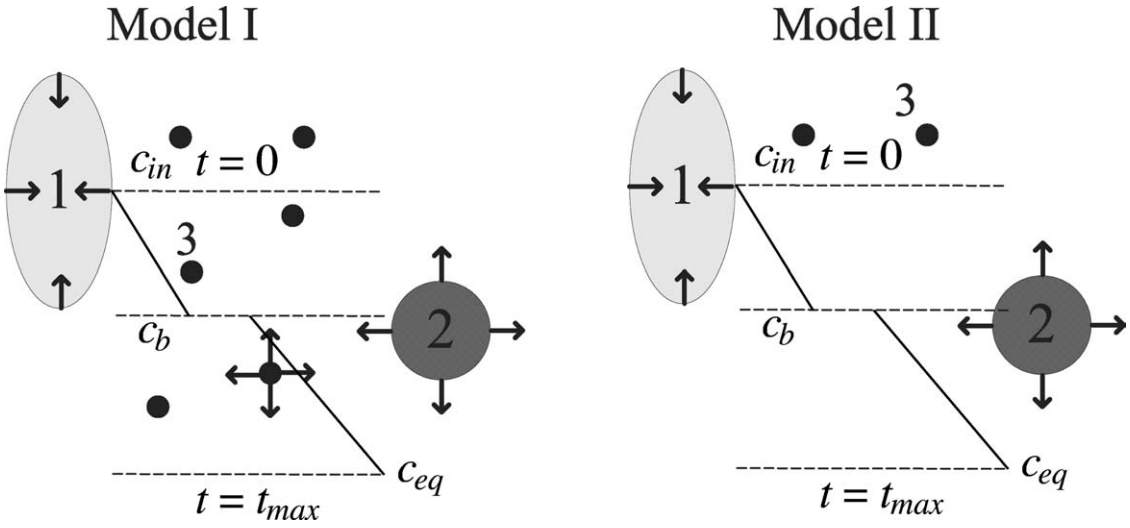

Figure 1. Gas hydrate nucleation and growth processes.

1: Contracting hydrate former droplet; 2: Expanding hydrate particle; 3: hydrate nuclei.

are sometimes in the PBM literature used only about the results of agglomeration and breakage not nucleation and growth. We use the terms about all the transitions, whatever their origin. Since its inception, PBM theory has developed to include the modelling of other particle properties in addition to size.[9]

A literature search for PBM modeling of gas hydrate particle size evolution reveals that the scope of knowledge in this field is not large at present.

Clarke and Bishnoi[10] used the PBM approach for estimating the surface area of gas-hydrate particles to calculate the rate of decomposition; a similar approach was used in the work of Hashemi and Macchi[11] to simulate gas hydrate growth in a stirred tank reactor. In both works modelling predictions were in agreement with experimental data. However, the only driving mechanism for "birth" and "death" events was considered to be particle decomposition/growth.

Taylor et al.[12] showed that hydrate particles may be cohesive and thus that growth/decomposition is not the only reason for change in the particle size. It was also shown in the work by Hounslow et al.[8] that, in addition to growth, flocculation and breakage as well as nucleation (formation of nano-sized nuclei) of cohesive particles are important for the correct prediction of their size. An important factor giving rise to aggregation and breakage aggregates are velocity fluctuations and shear present in the fluid.

Herri et al.[13] presented PBM-simulations for methane hydrate formation and further development in a water-gas stirred vessel. Hydrate particle nucleation and breakage were considered in combination with other governing mechanisms for the particle size evolution: secondary nucleation, aggregation, breakage, and attrition. It was found that the aggregation process is responsible for a higher rate of particle size increase than could be explained only on basis of the the growth process, even though the methane hydrate particles were found not to be very cohesive in water media. However, the flow field in their paper was considered to possess a spatially uniform shear rate which is not valid for the entire stirred vessel: the flow field fluctuations in the vicinity of the impeller are much more intensive than those in the bulk fluid. Kusters[14] in a detailed study of the flocculation of particles in similar system proposed several zones of turbulent intensities with different particle collision rates in each.

We conclude from this survey that there is a need for PBM models for hydrate particles in pipeline flow.

Objectives and Over-All Approach

The main objective of the present work is therefore to formulate a credible PBM-based model for pipeline flow of hydrates.

To achieve this, it is a sub-objective to formulate the necessary flow field parameters suitable for pumped pipe-line flow. These parameters will be different from those used in agitated vessels in the literature (see e.g., Ref. 13), and will involve formulating a two-compartment model to account for the very different flow fields in the pump and in the pipeline itself.

It is a further objective to validate and fine-tune the model by comparing it with experimental data from an appropriate system. These experimental data are found in literature[15] and used with kind permission of the authors.

Model Description

Nucleation and growth

In this work, we consider turbulent flow of a hydrate suspension in a recirculating loop. The continuous phase is water and there are two dispersed phases present: hydrate particles and hydrate former droplets. An isothermal process with thermodynamic parameters within the hydrate-stable region is considered, so that hydrate phase dissociation may be neglected. The process of hydrate formation is illustrated in Figure 1. When the hydrate-former is added to the flowing water it is dispersed into droplets due to shear forces acting on this second liquid phase. Initially, hydrate former diffuses into the bulk water phase resulting in a near-equilibrium

molar concentration of hydrate former, $l \times c_{in}$, in the bulk after sufficient time of hydrate former diffusion. Cages of crystal form around the hydrate former molecules thus forming hydrate nuclei, which are assumed to possess a negligibly small size.[1] After nuclei formation, the hydrate particles start to grow consuming hydrate former from the bulk and causing the volume concentration of hydrate particles to rise.

We call the concentration of hydrate former at the hydrate-former/bulk interface c_{in} and that at the bulk/hydrate-particle interface c_{eq}. The concentration in the bulk fluid, c_b, is initially, upon dispersion of the hydrate-former droplets in the bulk liquid at $t = 0$, close to c_{in}, but as the hydrate-particle/bulk interface grows due to continued nucleation and growth of hydrate particles the bulk concentration approaches c_{eq} and finally reaches c_{eq} at some time $t = t_{max}$ where the system has reached a steady state and the growth and nucleation of hydrate particles stop.

With respect to nucleation there are, according to the literature, two possible scenarios:

- Continuous production of hydrate nuclei until all the hydrate former is consumed.[16] This is Model I in Figure 1.
- Impulse initial nucleation, whereafter the dissolved hydrate former is preferentially consumed by the existing nuclei/particles for growth rather than for further nucleation.[17,18] This is Model II in Figure 1.

Summing up the aforementioned statements we formulate the PBM equations for these two different nucleation mechanisms assuming size-independent particle growth, G:[13]

$$\frac{\partial f}{\partial t} + G\frac{\partial f}{\partial r} = B_0\delta(r) \tag{1}$$

$$\frac{\partial f}{\partial t} + G\frac{\partial f}{\partial r} = 0 \tag{2}$$

so that $f(r,t)dr = N$, where N is the number of particles with radius between r and $r + dr$ in 1 m^3 of mixture. Equation 1 corresponds to Model I and Eq. 2 to Model II, respectively.

Initial conditions for Model I: $f(0,0) \cong 0$ assuming nuclei of zero size, and for Model II: $f(r_{in},0) = f_{in}$ with f_{in} obtained by linear fitting of the moments of the experimentally determined particle size distribution at the initial time. Nucleation and growth rates may be related to the hydrate former molar concentration according to Herri et al.[13] and Hounslow et al.[8] For the nucleation rate:

$$B_0 = k_1 \exp\left(-\frac{B}{\ln s}\right) \tag{3}$$

where B is a constant, $s = \overline{c_b}/c_{eq}$ is the relative supersaturation and $\overline{c_b}$ is the spatially averaged molar concentration of hydrate former in the bulk space of water. For the growth rate:

$$G = k_2\left(\overline{c_b} - c_{eq}\right) \tag{4}$$

The i'th moment of the particle size distribution (PSD), $f(r,t)$, is defined as:

$$M_i = \int_0^\infty r^i f(r,t)dr. \tag{5}$$

In the context of nucleation and growth the physical meanings of the four first moments of $f(r,t)$ are of particular importance for the present model. The zeroth moment is simply the total number of particles per m^3 in the system. The normalized first moment is the mean particle radius:

$$\bar{r} = \frac{M_1}{M_0}. \tag{6}$$

The second moment is proportional to a total area of particles per 1 m^3 of mixture with the proportionality coefficient 4π. The third moment is proportional to the volume concentration of particles in the system with the proportionality coefficient $4\pi/3$.[8] Equations 1 and 2 expand to two sets of ordinary differential equations by applying the moment transformation (Eq. 5) to them:

$$\frac{dM_0}{dt} = B_0 \tag{7a}$$

$$\frac{dM_i}{dt} = iGM_{i-1} \tag{7b}$$

$$\frac{dM_0}{dt} = 0 \tag{8a}$$

$$\frac{dM_i}{dt} = iGM_{i-1} \tag{8b}$$

where Eqs. 7a and 7b correspond to Model I and Eqs. 8a and 8b to Model II, respectively. Initial conditions for Model I: $M_i(0) = 0$, and for Model II: linear approximation of experimental data.

The two systems of Eqs. 7a, 7b, 8a, and 8b are not closed because of the unknown values of $\overline{c_b}$ and c_{eq}. They are to be quantified from experimental data.

Aggregation and breakage

When suspensions of sticky particles are sheared, e.g., in turbulent flow the particles may collide and produce aggregates leading to a decrease in the total number of particles and an increase in the mean particle size in the system. Conversely, when the turbulent fluctuations are of relatively high energy, aggregates may be destroyed due to the action of fluid shear or violent aggregate collisions. The total volume of particles is unchanged for both processes due to continuity.

To account for this Eqs. 7a–8b need to be extended to account for the "births" and "deaths" of particles due to aggregation and breakage:

$$\frac{dM_0}{dt} = B_0 + A_0 + \mathcal{B}_0 \tag{9a}$$

$$\frac{dM_i}{dt} = iGM_{i-1} + A_i + \mathcal{B}_i \tag{9b}$$

$$\frac{dM_0}{dt} = A_0 + \mathcal{B}_0 \tag{10a}$$

$$\frac{dM_i}{dt} = iGM_{i-1} + A_i + \mathcal{B}_i. \tag{10b}$$

The aggregation term for turbulent pipeline flow is calculated according to Randolph and Larson as a function of $f(V_p(r),t)$ and the particle collision rate[19] (dependence of variables on time is not shown):

$$A_i = \int_0^\infty r^i \cdot \left\{ \frac{1}{2} \int_0^{V_p} K(V_p - e, e)\, f(V_p - e) f(e) de - f(V_p) \cdot \int_0^\infty K(V_p, e) f(e) de \right\} dr. \quad (11)$$

The outer integration with the limits 0, ∞ on the right hand side is the moment transformation (Eq. 5) of the aggregation term, the first term of the aggregation term within the curly brackets represents the rate of increase in number of particles in the volume range V_p to $V_p + dV_p$ due to aggregation of particles smaller than V_p, the second term represents the rate of decrease of number of particles in the same size interval due to aggregation into larger particles, both divided by the interval width dV_p and both counted per unit volume of suspension.

$K(V_p,e)$ is the agglomeration kernel for particles with volumes V_p and e, respectively. This can for "orthokinetic" (shear-induced) agglomeration be modeled by the following expression due to Smoluchowski:[13,20,21]

$$K = \frac{4}{3} \gamma \alpha \left(V_{p,i}^{\frac{1}{3}} + V_{p,j}^{\frac{1}{3}} \right)^3 \quad (12)$$

where γ is the shear rate in the suspension and α is the collision efficiency, the fraction of collisions leading to agglomeration.

Equation 12 may be simplified assuming the collision rate of two particles to be independent of their size, and therefore the same as the collision rate of two particles both with the mean size, $\bar{r}$ (see e.g., De Boer et al.[22]):

$$K = \frac{4}{3} \gamma \alpha (2\bar{r})^3. \quad (13)$$

The collision efficiency α may be related to the ratio between flow shear force and the attractive van der Waals force:[20]

$$\alpha = k \left(\frac{H}{36 \pi \mu \gamma \bar{r}^3} \right)^{0.18}. \quad (14)$$

The value of the constant k depends, among other things such as the properties of the suspending fluid, on the particle size r. For example, in the work by van de Ven and Mason[20] k was determined to be equal 0.79, 0.87, 0.95 for particles of 2, 1, 0.5 μm, respectively assuming reasonable values for the suspending fluid properties.

The breakage term is calculated in a similar fashion to Eq. 11 (the dependence of the variables on time is not shown):

$$\mathcal{B}_i = \int_0^\infty r^i \cdot \left\{ \int_{V_p}^\infty \frac{2}{e} g(e) f(e) de - f(V_p) g(V_p) \right\} dr \quad (15)$$

where we have assumed a constant breakage function. The breakage rate g may be simplified by expressing it in the form of a power law as suggested by Spicer and Pratsinis,[21] but in addition using a size-independent formulation consistent with the treatment of agglomeration in Eq. 13:

$$g = k_4 \gamma^b \bar{r} \quad (16)$$

where the exponent b is a constant dependent on the floc tensile strength and k_4 is a proportionality constant obtained by fitting the model results to experimental data. Although the form of Eq. 16 is size-independent, the appearance of the mean particle size in the expression for g still ensures that breakage becomes more frequent if the size of the particles in the system increases.

Equations 11 and 15 may be integrated assuming some mathematical expression for $f(r,t)$. In the present model, we use the resulting expressions for A_i and $\mathcal{B}_i$ obtained by Herri et al.[13] assuming that $f(r)$ is a linear function of r in the form $f(r) = C_1(1 - r/C_2)$. The expression for the i'th moment of the aggregation term, A_i thus is:

$$A_i = J(i) K M_i M_0 \quad (17)$$

where $J(i)$ represents a series of constants, which can be expressed compactly as a sixth order polynomial in i with coefficients: -0.5, 0.001, -0.0145, 0.0798, -0.1962, 0.1722, 0.1957 in the order of increasing power of i from 0 to 6. The expression for the i'th moment of the breakage term, $\mathcal{B}_i$, is:

$$\mathcal{B}_i = k_4 \gamma^b (2^{1-i/3} - 1) M_{3+i}. \quad (18)$$

As the equation for the i'th moment thus contains higher-order moments of the particle size distribution in the breakage term, the systems of moment equations (Eqs. 9a–10b) are not closed. To close the equations the higher-order moments may be approximated as follows:[13]

$$M_i = r^{i-5} M_5, i > 5. \quad (19)$$

Determining the model parameters from experimental data

Quantifying the parameters involved in population balance analysis for particle size determination requires the knowledge of some hydrate physical properties, such as the particle Hamaker constant and the tensile floc strength, hydrate former mass transfer coefficient, and other. These properties are unavailable in literature for most types of hydrate. In this work, therefore, the model parameters are quantified by comparing experimental data to model results in order to determine those PBM parameters, which are based on these unknown material properties or relate to the physics of the process in some unknown way. These were k_1, k_2, B, $k_3 = k \cdot H^{0.18}$, k_4 and b. Most of these will be quantified by fitting

Table 1. Volume Fraction and Mean Particle Size As a Function of Time (Calculated from Wang et al.[15])

Time (s)	Volume fraction (%)	Mean particle diameter (μm)
7200	9.8	62.9
14,400	20.2	156.3
19,800	28.5	178.6

the model to experimental data as shown in the subsequent sections.

The experiment reported by Wang et al.[15] presents the history of formation and growth of hydrate particles in an HCFC hydrate slurry in a recirculating pipe-loop flow keeping the pump impeller at a fixed speed. The mean particle size (determined by sampling), the particle size distributions and the hydrate volume fraction, all as functions of time, in combination with calculated flow parameters for the experiment are used for quantification of the required PBM parameters below.

The volume fraction and mean particle diameter (determined by filtering samples through metal sizers) are shown as functions of time in Table 1 for the part of experiment of Wang et al.[15] before their first plugging event.

According to the description Wang et al.,[15] the initial amounts of hydrate former and water charged to the system were 44.8 kg and 170.4 kg, respectively, meaning that the initial concentration of hydrate former is $c_{\text{in}} = 1859.0$ mol/m^3, giving rise to 9.3 mol/m^3 of HCFC in the bulk since its solubility is $l = 5 \times 10^{-3}$. Most of the hydrate former available for dissolution and conversion into hydrate was consumed before the first plugging event (6.5 hrs after charging the system, as determined from Figure 4 in Ref. 15). We assume an exponential decrease of hydrate former concentration in the bulk liquid (Figure 1):

$$c_{\text{b}}(t) = l c_{\text{in}} \cdot \exp\left(-\frac{t}{t_{\max}}\right) \tag{20}$$

with the minimum value, c_{eq}, reached at $t = t_{\max}$:

$$c_{\text{eq}} = l c_{\text{in}} \cdot \exp(-1.0) \tag{21}$$

$t_{\max} = 6$ hrs $= 23{,}400$ s, the time at which the dissolved hydrate former concentration has decreased to the equilibrium value due to the consumption by the growing hydrate particles, was determined from experimental data[15] (Figure 4). Equations 20 and 21 are to be used as input to Model I (see later).

Equation 20 represents a simplification that makes the model much easier to evaluate. Formally the hydrate concentration in the bulk liquid should be calculated as a function of time using a mass balance equation for the bulk considering the feeding of hydrate former by dissolution from the dispersed droplets of pure hydrate former and the consumption of hydrate former by the forming hydrate particles. We did carry out such a calculation making reasonable assumptions about diffusion rates and the evolution of interfacial areas between the three phases, and found that Eq. 20 approximates the variation of the bulk concentration of hydrate former reasonably well. Details are available from the authors.

The experimental data shown in Table 1 represents almost linear increases in both volume fraction and diameter. To obtain initial values for the four first moments as input to Model II, straight lines through the origin were fitted to these data, and the values of volume fraction and mean diameter at 1/2 of the first time step read off. Knowing these two parameters and assuming the particles to be spherical allowed calculation of the first four moments listed in Table 2, which were used as input to Model II.

According to the experimental results of Wang et al.[15] (Table 1) the hydrate volume fraction increased almost linearly with time. Thus, the time derivative of the third moment of particle size distribution may be derived as follows:

$$\frac{dM_3}{dt} = 2 \cdot G M_2 = S. \tag{22}$$

For Model II the growth rate can be derived directly from experimental data:

$$G = \frac{S}{4\pi M_2} \tag{23}$$

where $S = 1.005 \times 10^{-5}$ 1/s is derived from the Table 1.

Particle aggregation and growth terms require the shear rate to be determined. In this work, we are modelling a flow loop which consists of two regions: a pipeline and a pump region. In the pipeline region average flow parameters are considered, possible local disturbances, such as bends, valves, flanges, fittings and sensors, are not considered and the pipeline region is assumed to be long enough to obtain fully developed turbulent flow after the disturbance introduced by the pump. The shear rate induced in a fully developed turbulent flow is calculated according to the relation by Kolmogorov:[23]

$$\bar{\gamma}_p = \sqrt{\frac{\bar{\epsilon}}{\nu_{\text{w}}}} \tag{24}$$

where the turbulent energy dissipation rate ε for the pipeline flow may be calculated from:[23]

$$\bar{\epsilon}_p = \frac{v}{\rho_{\text{w}}} \frac{dP}{dL} \tag{25}$$

where in the experiments the mean velocity, $v = 1$ m/s, and $\frac{dP}{dL} = 291.6$ kPa/m.[3,15] The mean shear rate in the pipeline thus comes to $\bar{\gamma}_p = 540$ s^{-1}.

The shear rate in the pump, close to the blades of the impeller, is calculated using Kármán theory,[24] which has been confirmed experimentally for a centrifugal pump by Lutz et al.:[25]

Table 2. Initial Moments of Particle Size Distribution (Input to Model II)

i	Moment	
0	2.9×10^{13}	m^{-3}
1	9.3×10^{7}	m^{-2}
2	18.6	m^{-1}
3	3.6×10^{-4}	–

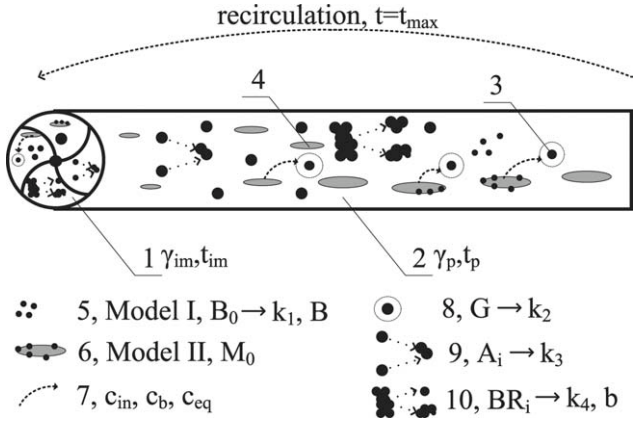

Figure 2. Illustration of the physical processes included in the present model.

1: Pump compartment; 2: Pipeline compartment; 3: Hydrate particle/nuclei; 4: Hydrate former bubble; 5: Continuous nucleation; 6: Impulse nucleation; 7: Hydrate former diffusion; 8: Hydrate particle growth; 9: Particles aggregation; 10: Aggregate breakage.

$$\bar{\gamma}_{im} = 6.3\bar{\omega}Re^{0.5} \tag{26}$$

where $Re = \bar{\omega}D^2\rho_w/\mu_w$, $D = 0.085$ m and $\bar{\omega} = 3.8\,1/\text{s}$. The mean shear rate in the pump $\bar{\gamma}_{im} = 3975\,1/\text{s}$. The present model does not account for mean shear rate changing due to increase in the slurry rheology.

The precise way of using the aforementioned equations is described in the subsequent section.

Numerical solution

The physical processes involved in the present model are presented in Figure 2. The system pump/pipeline is divided into two separate compartments[14] with different shear rates $\bar{\gamma}_p$ (Eq. 24) and $\bar{\gamma}_{im}$ (Eq. 26), and different residence times $t_p = F/V_p = 29.7$ s and $t_{im} = F/V_{im} = 1.62$ s.

For Model I the solution steps are (see also the illustrations in Figure 2):

1. calculation of the hydrate-former equilibrium molar concentration c_{eq} (Eq. 21)
2. external input of nucleation, growth, aggregation and breakage constants and parameters (k_1, k_2, B, k_3, k_4, b)
3. calculation of the current system time
4. calculation of the current molar concentration in the bulk c_b (Eq. 20)
5. calculation of nucleation and growth rates, B_0 and G, respectively (Eqs. 3 and 4)
6. calculation of aggregation A_i and breakage terms $\mathcal{B}_i$ (Eqs. 17 and 18, respectively)
7. solution of Eqs. 9a and 9b by the fourth-order Runge-Kutta technique[26] with a time step of 0.1 ms. The solution is found within one of the two compartments using the appropriate residence time (t_p or t_{im})
8. input of the computed moments for one compartment to the next compartment (recirculation)
9. repeat the operations in 3–8 until the simulation time has become equal to the duration of the experiment to be modeled (Table 1)
10. compare model results with experimental data and repeat the operations in points 2–9 to obtain an optimal fit to experimental data.

For Model II the solution steps do not require the calculation of hydrate former properties. The steps are:

1. input of initial PSD moments from Table 2
2. external input of aggregation and breakage constants and parameter (k_3, k_4, b)
3. calculation of the current system time
4. calculation of growth rate G (Eq. 23)
5. calculation of aggregation and breakage terms, A_i and $\mathcal{B}_i$ (Eqs. 17 and 18, respectively)
6. solution of Eqs. 10a and 10b by the fourth-order Runge-Kutta technique[26] with a time step of 0.1 ms. The solution is found within one of the two compartments using the appropriate residence time (t_p or t_{im}).

The remainder of the Model II solution algorithm is the same as for Model I.

Results and Discussion

Growth and nucleation

Equations 9a–10b show that the nucleation and growth rate terms are responsible for the development of the third moment of the particle size distribution with time. Preliminary simulations including all mechanisms confirmed that aggregation and breakage did not play a significant role during the initial stages of the process. This also stands to reason, since the particles initially are small, leading to negligible breakage, and very dilute, leading to negligible aggregation. We therefore chose to neglect aggregation and breakage when fitting the growth and nucleation constants to the experimental data from the initial stages of the process.

The total number of hydrate particles depends on the nucleation rate (Eqs. 9a–9b) so the mean particle size (Eq. 6) is also a function of B_0. Thus, the nucleation and growth rate constants can be quantified in Model I by optimizing the fit between the simulated diameter and volume-fraction variations in time (neglecting, as mentioned earlier, aggregation and breakage) with those found experimentally. The optimization criterion: the longest temporal fit to experiment for the diameter and volume fraction. The values found in this way were: $k_1 = 2.5 \times 10^{10}$ m^{-3} s^{-1}, $k_2 = 1.3 \times 10^{-9}$ m^4/s mol, $B = 5.0$.

For Model II no fitting of these parameters is necessary, since the particle growth rate (Eq. 23) and the initial number of zero-sized particles (Table 2) have already been calculated directly from the experimental data.

Simulation results for hydrate volume fraction and mean particle diameter as functions of time for Models I and II are compared with experimental data in Figures 3 and 4; aggregation and breakage terms are neglected. It is seen in Figure 3 that for Model I the hydrate-phase volume fraction increase is less than that found experimentally during the early stages of the process (up to the first experimental point). This is explained by the continuous-nucleation assumption whereby the nuclei available for further growth are produced continuously so that, in order not to overpredict the last experimental result, the initial nucleation did not produce enough zero-sized particles to fit the experimental

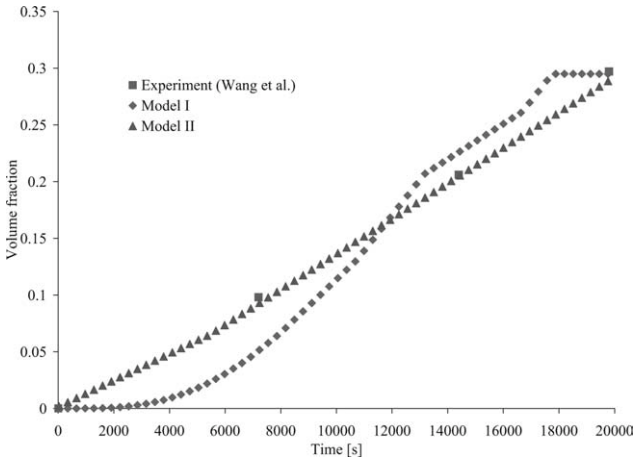

Figure 3. Hydrate volume fraction as a function of time.

Model I and Model II results are compared with experimental data.[3] $k_1 = 2.5 \times 10^{10}$ m^{-3} s^{-1}, $k_2 = 1.3 \times 10^{-9}$ m^4/s mol, $B = 5.0$. Aggregation and breakage terms are neglected.

volume fraction, even with a relatively large growth-rate constant (see Figure 4). As a significant part of hydrate former becomes consumed, the rate of increase in volume fraction predicted by Model I is reduced as a consequence of the decrease in the growth rate due to a reduction in the bulk concentration of the hydrate former. At this stage, Model I is seen to overpredict the volume fraction slightly. When finally, somewhere between 16,000 and 18,000 s, the molar concentration of the hydrate former in the bulk approaches its equilibrium value Model I predicts no further growth.

Model II, on the other hand (Figure 3) agrees rather closely with the experimental data and predicts a linear increase in the volume fraction over the entire simulation time.

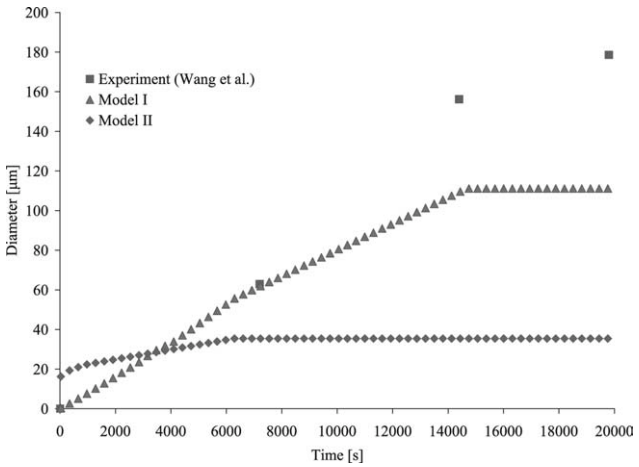

Figure 4. Mean particle diameter as a function of time.

Model I and Model II results are compared with experimental data.[3] $k_1 = 2.5 \times 10^{10}$ m^{-3} s^{-1}, $k_2 = 1.3 \times 10^{-9}$ m^4/s mol, $B = 5.0$. Aggregation and breakage terms are neglected.

The differences in optimization strategy for the two models can be seen in Figure 4: the constants for Model I were selected in a way so the model simulation matched the experimentally determined particle size as long as possible, Model II is a volume-fraction-history fit so the mean particle diameter could not be changed independently. The time-mean growth rate for Model I was thus set to be larger than for Model II for two reasons: the different optimization strategies and the continuous nucleation in Model I, which is responsible for holding the mean particle size down, opposing the effect of particle growth (Eq. 6).

Beyond around 8000–10,000 s, both Model I and Model II can be seen in Figure 4 to significantly underpredict the mean particle diameter compared with experiment. This is probably due to particle aggregation having been neglected. Thus, the usage of an aggregation term (and a breakage term) is required for the complete simulation of experiment.

The expression presented in Eq. 3 assumes a certain value of supersaturation at which nucleation stops. From Figure 5 it can be seen that $B = 5.0$ corresponds to the nucleation stopping after ~2200 s, having a limit at the supersaturation value of 2.15. Decreasing the value of B shifts the limiting supersaturation to lower values, prolonging the nucleation process in time. The use of a lower value for B would result in the use of larger growth rate constant k_2 when fitting the Model I results to experimental data because of the increased amount of submicron particles in the PSD.

Aggregation and breakage

Simulation results for the particle diameter as a function of time for Model I and Model II with incorporated aggregation and breakage terms are presented in Figure 6 and compared with experimental data.[3]

We first focus on Model I. It can be seen that during the initial phase the Model I results are quite similar to those produced by Model I when including only the nucleation and growth terms (Figure 4). The difference begins after the time corresponding to the first experimental point, at which the particle size is 62.9 μm. This point in time may therefore

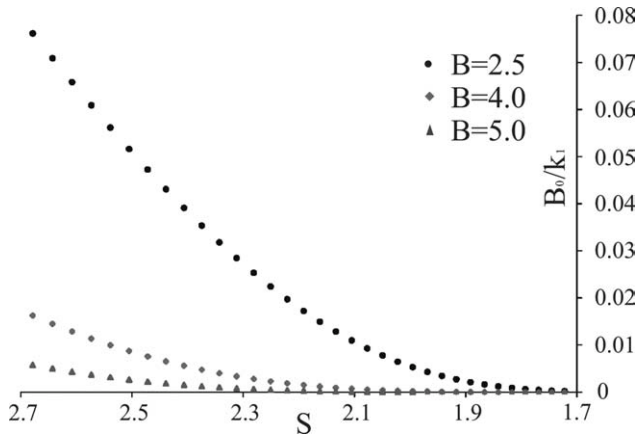

Figure 5. Nucleation rate scaled with the nucleation rate constant k_1 as a function of relative supersaturation for different nucleation parameters.

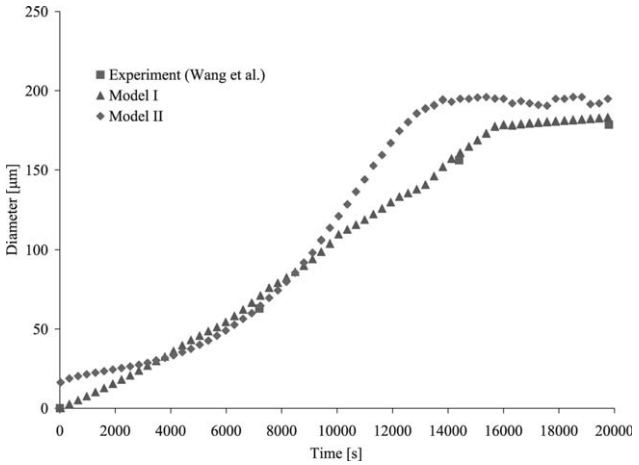

Figure 6. Mean particle diameter as a function of time including aggregation and breakage terms.

Model I and Model II results are compared with experimental data.[3] Model parameters are given in Table 3.

be surmised to be the time at which particle agglomeration and breakage become important and the particle size of 62.9 μm can therefore be taken to represent the size of a particle, which is primary from the aggregation and breakage point of view (hereinafter referred to as a "primary particle").

After this point the Model I particle diameter in Figure 6 becomes significantly higher than that in Figure 4 due to aggregation. Finally, when the diameter approaches 178 μm, the breakage becomes more important and the particle size reaches an approximately steady size of around 183 μm.

The aggregation and breakage constants obtained as a result of fitting the Model I results to experimental data are presented in Table 3. The aggregation constant, k_3, found to be optimal produces relatively low collision efficiencies of the 4th order of magnitude which are similar to the values obtained by Herri et al.[13] for methane hydrate particles in a stirred vessel in water. The breakage constant, k_4, and parameter b are similar to those obtained by L. Wang et al.[27] in their study of the aggregation and breakage of latex spheres in laminar Couette flow.

The Model II results are similar to those of Model I until the time corresponding to the first experimental point (when the "primary particle" size has been reached), but after that they are significantly different; the aggregation appears to be more intensive than in Model I. This is due to larger volume fraction of hydrate particles (see Figure 4 and below). The particle diameter approaches the steady value ($\sim$188 μm, similar to that of Model I) faster and the steady period for Model II is therefore longer. The discrepancy with experiment for mean particle diameter (Figure 4) for Model II is larger than that for the Model I output. This may be explained by more significant change in the slurry rheology (larger volume fraction) which is not accounted for in the model.

Table 3. Aggregation and Breakage Constants Obtained by Fitting Model I and Model II Results to Experimental Data

Parameter	Model I	Model II	
k_3	3.88×10^{-8}	3.12×10^{-8}	$J^{0.18}$
k_4	1100.0	800.0	s^{b-1}/m^3
b	1.89	1.90	

The aggregation constant found by fitting the Model II results to experiment (Table 3) is similar to, but slightly lower than, that used in Model I. This is due to larger volume fraction of hydrate which leads to more intensive aggregation. The breakage exponent b for Model II is slightly larger than that for Model I, which, in combination with lower k_4, gives a weaker breakage term. The collision efficiencies (Eq. 14) for Model II are also of the 4th order of magnitude.

We continue this section with a discussion of some features of the two-compartment model used in this work. The fluid-particle interaction is different for pipeline and pump compartments due to the different shear rates there. A series of additional simulations were conducted in order to illustrate the development of the mean particle size in time due to aggregation and breakage in both compartments independently. To do this, the nucleation and growth terms were neglected and Eqs. 7a and 7b were solved with a fourth-order Runge-Kutta technique,[26] using arbitrarily selected initial PSD moments.

Figure 7 presents the simulation results for the particle-size history in the pump and pipeline compartments independently. The initial median particle diameter was set to 60 μm, the particle size distribution was assumed to be log-normal with the standard deviation of 1.2 and the volume fraction of particles was set to 10%. It can be seen from the Figure 7 that during the initial stages of the process the aggregation is the dominant mechanism in both compartments, and the aggregation in the pump is the more intensive due to the almost 8 times larger shear rate there. Once the particle size becomes large enough ($\sim$2 times and 5 times larger than the initial size in the pump and pipeline compartments, respectively) the aggregation is compensated by the breakage so the particle size reaches steady values. The steady value in the

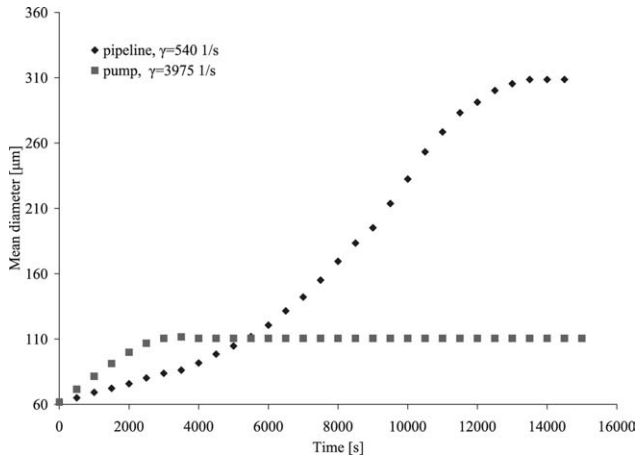

Figure 7. Mean particle diameter as a function of time for the two separate compartments.

The aggregation and breakage parameters are those used for Model II in the previous sections (Table 3). Initial median particle diameter: 60 μm; initial particle size distribution: log normal with a standard deviation of 1.2; hydrate phase volume fraction 10%.

Table 4. Percentage Deviation in the Model Outputs Due to Halving and Doubling the Process Parameters Relative to Those Determined by Fitting to Experimental Data

Parameter		Volume Fraction		Mean Diameter	
Model I	Model II	Model I	Model II	Model I	Model II
$k_1 = 1.25 \times 10^{10}$	$M_0 = 1.45 \times 10^{13}$	−46	−2	−11	−20
$k_1 = 5.00 \times 10^{10}$	$M_0 = 5.80 \times 10^{13}$	+106	+2	+27	+35
$k_2 = 6.50 \times 10^{-10}$	$S = 5.00 \times 10^{-6}$	−84	−48	−55	−15
$k_2 = 2.60 \times 10^{-9}$	$S = 2.01 \times 10^{-5}$	+76	+108	+45	+10
$k_3 = 1.94 \times 10^{-8}$	$k_3 = 1.56 \times 10^{-8}$	–	–	−11	−24
$k_3 = 7.76 \times 10^{-8}$	$k_3 = 6.24 \times 10^{-8}$	–	–	+30	+57
$k_4 = 550$	$k_4 = 400$	–	–	+10	+11
$k_4 = 2200$	$k_4 = 1600$	–	–	−2	−6

pump is reached much faster in the pump than in the pipeline, but is much lower. These results are reasonable.

We briefly report on the sensitivity of the model predictions for volume fraction and mean particle size to variations in the model parameters. The effects of halving and doubling the model parameters relative to those obtained by fitting are shown in Table 4 (Model II constants, modified in this way, are not presented in the Table).

The variations of both volume fraction and mean particle size with the modified constants were qualitatively the same for both models as those in Figures 3 and 6. Differences were only observed in the slopes and the absolute values.

A change of nucleation constant in Model I causes an almost proportional change in hydrate volume fraction output, and causes the diameter to change within a 40% interval. Model II is not sensitive to the initial amount of particles in terms of volume fraction because of its specific growth rate expression (Eq. 23); this makes the diameter more strongly dependent on the initial amount of nuclei. The influence of the nucleation parameter B on Model I is similar to that of k_1 and is not presented here.

Varying the growth rate constant k_2, in turn, causes an almost proportional change in to the mean particle size while the volume fraction changes as the third power of the constant due to the linearity of the growth rate. Conversely, the growth rate coefficient in Model II influences the volume fraction linearly while the effect on the mean diameter is weaker (within 20%).

The aggregation and breakage processes do not impact the predicted volume fraction. Variation in the aggregation constant significantly impacts the predictions of both models. The response of Model II to the variation in k_3 is ~20% stronger than that of Model I due to the larger volume fraction and smaller breakage constant. The influence of the breakage constant k_4 is less than that of k_3 due to the influence of growth; the two models react almost identically to variations in k_4. The influence of the breakage exponent b is qualitatively the same as for k_4.

Both models show negligible sensitivity (less than ±2%) to variations in the time step within an interval 0.05 ms < dt < 0.2 ms.

Particle size distribution

Unnormalized particle size distributions are available from the experimental results of Wang et al.[3] for the three hydrate-phase volume fractions of 9.8, 20.2 and 28.5%. To compare them with the results from our model, these experimental distributions were normalized using the trapezoidal rule. The use of metal sizers with lower limit of 74 μm^3 for particle size determination provides a rather coarse estimation of the particle size distribution because submicron particles produced in a nucleation process could not be distinguished. However, the available sampling results are presented in the article for process times greater than 2200 s at which the nucleation stops. Thus, in the current work we assume the amount of submicron particles to be negligibly low compared to the amount of particles of several microns due to the growth and aggregation. In this way, the points (0,0) and the last point of the 28.5% distribution were assumed for our normalization of the data.

We use the moments output from our PBM model to calculate equivalent log-normal particle size distributions.

The parameters σ and d_m in the log-normal distribution function:

$$\frac{1}{x\sigma\sqrt{2\pi}}\exp\left[-\frac{(\ln(x)-\ln(d_m))^2}{2\sigma^2}\right] \tag{27}$$

may be calculated from the moments of the distribution:

$$\widetilde{M}_i = \exp\left[i\ln(d_m) + i^2\frac{\sigma^2}{2}\right] \tag{28}$$

from the following formulae:

$$\sigma = \left(\ln\left[\frac{\widetilde{M}_2}{\widetilde{M}_1^2}\right]\right)^{0.5} \tag{29a}$$

$$d_m = \widetilde{M}_1 \exp[-0.5\sigma^2]. \tag{29b}$$

This can be done using the output moments from our model, we need to normalize the output moments:

$$\widetilde{M}_i = \frac{M_i}{M_0}, \tag{30}$$

since the zeroth moment in the PBM model is not unity, as it is in the log-normal distribution, which is a probability density function, but represents the number of particles per m^3 in the system.

The particle size distributions calculated from the results of Model I in this way are compared with the experimental data in Figures 8–10.

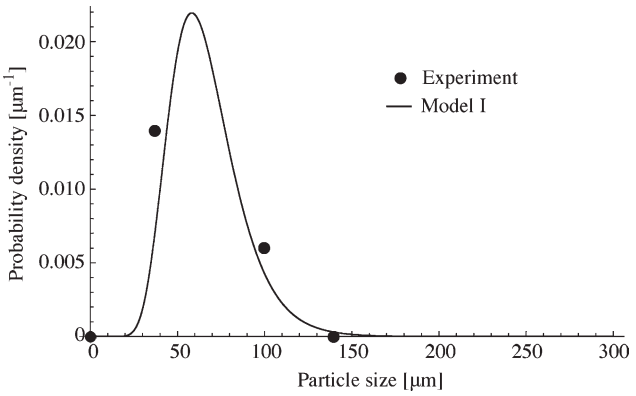

Figure 8. Particle size distribution.

Hydrate volume fraction 9.8% (7200 s). Model I results are compared with the experimental data.[3]

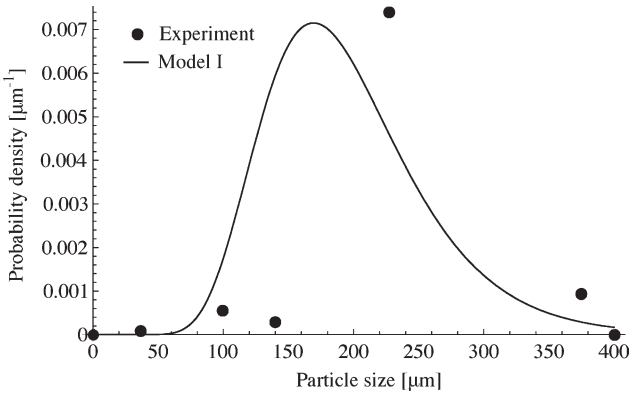

Figure 10. Particle size distribution.

Hydrate volume fraction 28.5% (19,800 s). Model I results are compared with the experimental data.[3]

We see that the agreement is quite good for the hydrate volume fractions of 9.8% and 28.5% in Figures 8 and 10, respectively, although the model distribution is slightly finer in the latter.

For the hydrate volume fraction 20.2% (Figure 9) the model distribution is much narrower than the experimental distribution. The parameter determining the spread, sigma, is also much smaller in this distribution than in the two others. This discrepancy may be partly due to an artifact of the model, and partly due to the experimental distribution appearing wider than it is, e.g., that the right zero-point of the distribution is at a lower value than the last experimental point of 375 μm.

One feature that the assumption of log-normal distributions cannot account for is the experimentally observed[3] bimodality in some of the the PSDs.

Conclusions

A computational study of the development of the size of hydrate particles in recirculating system with turbulent slurry pipe flow has been carried out and validated with experimental data from the literature. The model was based on a two-compartment system, which allowed us to account for the difference in shear rate between the pump and the pipeline.

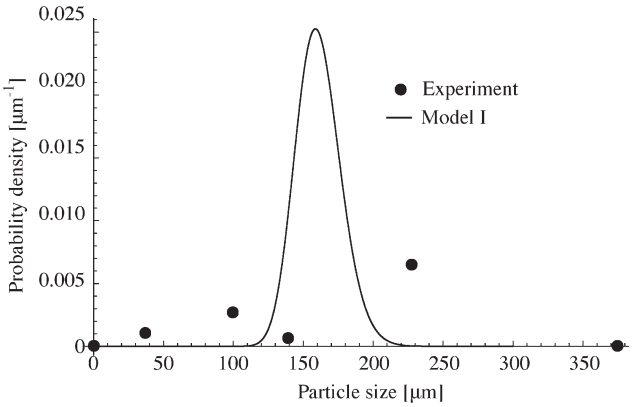

Figure 9. Particle size distribution.

Hydrate volume fraction 20.2% (14,400 s). Model I results are compared with the experimental data.[3]

The simulation results were validated with experimental data available in literature[15] for a recirculating low-pressure hydrate flowloop. It was shown that interactions of particles (aggregation and breakage) are likely to influence the mean particle size significantly and that the effects of these interactions are comparable to the effects of growth and nucleation. During the validation with experimental[15] data it was further found that HCFC hydrate particle coagulate in turbulent water flow with relatively low collision efficiencies and the aggregate strength parameters were found to be comparable to the ones determined in the work by L. Wang et al.[27] for latex spheres in Taylor-Couette flow.

Two different approaches for hydrate nucleation and growth modeling were used in order to compare the aggregation and breakage parameters resulting from fits to the experimental data, one with continuous nucleation during the process, and another with only an initial pulse nucleation. The aggregation and breakage parameters were found to be very similar between the two models.

The combination of both approaches for nucleation and growth into one joint model is also possible and would reproduce a process with a large initial nucleation pulse and continuous secondary nucleation over the entire process. Having more particles than either in Model I or Model II, due to both types of nucleation process being active, and fitting the model results to experimental data for hydrate phase volume fraction would result in a lower growth rate in the system resulting in smaller primary particles. The aggregation of smaller particles would likely be more effective even at the rates determined in the current work, so the aggregation constant could expected to be of the same order of magnitude as we obtained. The breakage parameters would probably be slightly greater then those used in the current work compensating for the enhanced aggregation. It is possible that such an approach may allow somewhat better fitting to the experiment results.

A reconstruction of log-normal particle size distributions from the computed PBM moments was presented and compared to the experimental data. Predictions for two of the three cases are in good agreement with experiment while the third seems to be much narrower than the experimental distribution.

Acknowledgments

The authors gratefully acknowledge StatoilHydro, Chevron ETC, SINTEF Petroleum Research, and the Norwegian Research Council for funding and for permission to publish the data shown in this article. The special acknowledgments are addressed to Dr. Shuanshi Fan from Guangzhou Center for Gas Hydrate Research for the permission to use his data in the present work.

Notation

A_i = i^{th} moment of the aggregation term (m^{i-3}/s)
b = breakage exponent
B = nucleation parameter
B_0 = nucleation rate ($m^{-3}s^{-1}$)
$\mathcal{B}_i$ = i^{th} moment of the breakage term (m^{i-3}/s)
c = molar concentration (mol/m^3)
d = particle diameter (m)
D = diameter of pump impeller (m)
f = unnormalized particle size distribution function (m^{-4})
F = volumetric flow rate (m^3/s)
G = growth rate (m/s)
g = breakage function ($m^{-2}\ s^{-1}$)
H = Hamaker constant (J)
k = collision efficiency prefactor
k_1 = nucleation rate constant ($m^{-3}\ s^{-1}$)
k_2 = growth rate constant ($m^4/s\ mol$)
k_3 = aggregation constant ($J^{0.18}$)
k_4 = breakage constant (s^{b-1}/m^3)
K = rate of collisions (m^3/s)
l = HCFC dissolution coefficient
L = length of the pipeline (m)
M_i = i-th moment of particle size distribution function $f(r,t)$ (m^{i-3})
$\widetilde{M}_i$ = i-th moment of normalized particle size distribution function (m^i)
p = pressure (Pa)
r = particle radius (m)
Re = Reynolds number
s = relative supersaturation
S = slope of linear approximation of experimental data (s^{-1})
t = time (s)
v = mean flow velocity (m/s)
V = volume (m^3)

Greek letters

α = collision efficiency constant
$\delta(r)$ = Dirac function (m^{-1})
ε = energy dissipation rate per unit mass (m^2/s^3)
ϕ = volume fraction
γ = shear rate (s^{-1})
μ = dynamic viscosity (Pa s)
ν = kinematic viscosity (m^2/s)
ω = frequency (s^{-1})
ρ = density (kg/m^3)

Subscripts and superscripts

eq = equilibrium condition
in = initial condition
b = bulk space
i = number of particle size distribution moment
max = maximum
im = pump impeller
p = pipeline
w = water
= spatial averaging

Literature Cited

1. Sloan ED, Koh CA. *Clathrate Hydrates of Natural Gases*, 3rd ed. Boca Raton, FL: CRC Press, 2008.
2. Sloan ED. Fundamental principles and applications of natural gas hydrates. *Nature*. 2003;426:353–363.
3. Wang W, Fan S, Liang D, Yang X. Experimental study on flow characters of CH3CCl2F hydrate slurry. *Int J Refrig*. 2008;31:371–378.
4. Hiroshi K. Natural gas transportation by methane hydrate. *Techno Mar*. 1999;842:586–594.
5. Aliev AM, Yu. Yusifov R, Kuliev AR, Yu. Yusifov G. Method of gas hydrate formation for evaluation of water desalination. *Russ J Appl Chem*. 2008;81:588–591.
6. Darbouret M, Cournil M, Herri J-M. Rheological study of TBAB hydrate slurries as secondary two-phase refrigerants. *Int J Refrig*. 2005;28:663–671.
7. Sinquin A, Palermo T, Peysson Y. Rheological and flow properties of gas hydrate suspensions. *Oil Gas Sci Technol*. 2004;59:41–57.
8. Hounslow MJ, Ryall RL, Marshall VR. A discretized population balance for nucleation, growth, and aggregation. *AICHE J*. 1988; 34:1821–1832.
9. Ramkrishna D. *Population Balances, Theory and Applications to Particulate Systems in Engineering*. San Diego, CA: Academic Press, 2000.
10. Clarke M, Bishnoi PR. Determination of the intrinsic rate of gas hydrate decomposition using particle size analysis. *Ann NY Acad Sci*. 2006;912:556–563.
11. Hashemi S, Macchi A. Gas hydrate growth model in a semibatch stirred tank reactor. *Ind Eng Chem Res*. 2007;46:5907–5912.
12. Taylor CJ, Dieker LE, Miller KT, Koh CA, Sloan ED Jr. Micromechanical adhesion force measurements between tetrahydrofuran hydrate particles. *J Colloid Interface Sci*. 2007;306:255–261.
13. Herri JM, Pic JS, Gruy F, Cournil M. Methane hydrate crystallization mechanism from in-situ particle sizing. *AICHE J*. 1999;45:590–602.
14. Kusters KA. The influence of turbulence on aggregation of small particles in agitated vessels. *PhD thesis*. Technische Universiteit Eindhoven, Eindhoven, Netherlands, 1991.
15. Wang W, Deqing L, Fan S. Formation and blockage of HCFC-141B hydrate in pipeline. In: Austvik T, Collett TS, Englezos P, Mehta A, Paull CK, Ripmeester J, Sloan ED, Uchida T, editors, *Proceedings of the 6th International Conference on Gas Hydrates (ICGH 2008)*, Vancouver, BC, Canada, 2008, pp. 1–6 (Session p-4).
16. Jones AG, Hostomsky J, Li Z. On the effect of liquid mixing rate on primary crystal size during the gas-liquid precipitation of calcium carbonate. *Chem Eng Sci*. 1992;47:3817–3824.
17. Vysniauskas A, Bishnoi PR. A kinetic study of methane hydrate formation. *Chem Eng Sci*. 1983;38:1061–1072.
18. Vysniauskas A, Bishnoi PR. A kinetic study of methane hydrate formation. *Chem Eng Sci*. 1985;40:299–303.
19. Randolph AD, Larson MA. *Theory of Particulate Processes*. St. Louis, MO: Academic Press, 1972.
20. van de Ven TGM, Mason SG. The microrheology of colloidal dispersions. VII. Orthokinetic doublet formation of spheres. *Colloid Polym Sci*. 1977;255:468–479.
21. Spicer PT, Pratsinis SE. Coagulation and fragmentation: universal steady-state particle-size distribution. *AICHE J*. 1996;42:1612–1620.
22. De Boer GBJ, Hoedemakers GFM, Thoenes D. Coagulation in turbulent flow. Part I. *Chem Eng Sci*. 1989;67:1821–1832.
23. Heath AR, Bahri PA, Fawell PD, Farrow JB. Polymer flocculation of calcite: experimental results from turbulent pipe flow. *AICHE J*. 2005;52:1284–1293.
24. Wichterle K, Sobolik V, Lutz M, Denk V. Shear rate on centrifugal pump impeller. *Chem Eng Sci*. 1998;1996:5227–5228.
25. Lutz M, Denk V, Wichterle K, Sobolik V. Electrodiffusional flow diagnostics in a centrifugal pump. *J Appl Electrochem*. 1998; 28:337–342.
26. Butcher JC. *Numerical Methods For Ordinary Differential Equations*. Bognor Regis: John Wiley and Sons, 2003.
27. Wang L, Marchisio DL, Vigil RD, Fox RO. CFD simulation of aggregation and breakage processes in laminar Taylor-Couette flow. *J Colloid Interface Sci*. 2005;282:380–396.

Manuscript received July 13, 2009, and revision received Oct. 16, 2009.